ISSN 1027-4510, Journal of Surface Investigation. X-ray, Synchrotron and Neutron Techniques, 2007, Vol. 1, No. 1, pp. 1–6. © Pleiades Publishing, Ltd., 2007.
Original Russian Text © A.A. Snigirev, V.G. Kohn, E.Kh. Mukhamedzhanov, I.I. Snigireva, A.G. Maevskii, V.V. Kvardakov, M.V. Kovalchuk, 2007, published in Poverkhnost'. Rentgenovskie, Sinkhrotronnye i Neitronnye Issledovaniya, No. 1, pp. 3–9.

Source Focusing and Coherent Imaging of a Microscopic Object at Weak Spatial Coherence of the Synchrotron Radiation Beam

A. A. Snigirev[a], V. G. Kohn[b], E. Kh. Mukhamedzhanov[b], I. I. Snigireva[a], A. G. Maevskii[b], V. V. Kvardakov[b], and M. V. Kovalchuk[b]

[a] *European Synchrotron Radiation Facility, BP 220, F-38043 Grenoble Cedex, France*

[b] *Russian Research Center Kurchatov Institute, pl. Kurchatova 1, Moscow, 123182 Russia*

Received December 30, 2005

Abstract—Experimental results are presented on the measurement of a holographic (phase-contrast) image of a boric fiber (100-μm-diameter boric cylinder with a 20-μm-diameter tungsten core) and on radiation focusing by Fresnel zone plates using the Kurchatov synchrotron radiation source. By comparison of the obtained hologram with theoretically calculated data, the vertical size of the source was determined to be 325 ± 25 μm. This value was also confirmed by measuring the half-width of the direct image of the source. Features of image recording on a photographic film are discussed.

DOI: 10.1134/S1027451007010016

INTRODUCTION

In 1995, after the advent of synchrotron radiation sources of the third generation (ESRF, APS, and Spring-8), it was found that these sources produce x-ray beams with high spatial coherence, close to laser beams in their parameters. This fact led to the emergence of new fields of x-ray optics, such as the direct high-resolution phase-contrast near-field imaging of microobjects [1, 2] and the holographic recording of microobject images, followed by reconstruction of the total optical density from the beam direction using numerical methods [3]. The additional use of conventional tomography methods allowed the optical density to be reconstructed in the cross section of a weakly absorbing object, when the absorbance varies at the noise level and cannot be used in analysis. The angular size of new sources in the object exposure region is on the order of 10^{-6} rad, which is comparable to or even higher than the resolution achieved using crystals. New sources made it possible to obtain x-ray beams of extremely small sizes by focusing the diverging wave by various x-ray lenses, among which Bragg–Fresnel lenses [4], Fresnel zone plates (ZPs) [5, 6], and compound refractive lenses [7, 8] are of most interest. Recently, refractive lenses of various types have been actively developed, and more than a hundred papers on this problem have been published up to the present. These lenses, as well as ZPs, do not change the optical axis direction. They have a single focusing order, which makes these lenses of primary importance for the development of x-ray microscopes. Beams with transverse sizes of the order of 100 nm [9] and ten times magnified high-contrast images of weakly absorbing biological microobjects [10] have been already obtained.

An obvious and important problem is the development of methods for the precise determination of the effective source size, since the coherent wavefront structure in practical experiments can be distorted by various optical elements placed in the source-to-object path, e.g., a monochromator. Moreover, the effective size is affected by various mechanical instabilities. The effective source size can be determined both by focusing and by analyzing interference fringes in holographic images of model objects [11, 12]. The problem of possible, at least partial, extension of the field of application of new methods to second-generation sources, which number in the tens in the world, also seems natural.

In this study, we have analyzed a number of the capabilities of second-generation sources for the practical use of spatially coherent phenomena, even under conditions of a significant loss of coherence. The experiment was carried out at the source of the Kurchatov Center for Synchrotron Radiation and Nanotechnology (KCSRNT). Since this SR source was not previously applied to such problems, the first objective was the determination of its effective transverse size. Two methods were used to solve this problem: source focusing by a Fresnel ZP and recording the holographic image of a thin boric fiber. The vertical (minimum) source size was estimated from an analysis of the experimental data obtained by these two methods. In the next section, we describe the experimental layout and present the experimental data. In the third section, we analyze the experimental results, and the fourth section is devoted to particular details of the used measurement method.

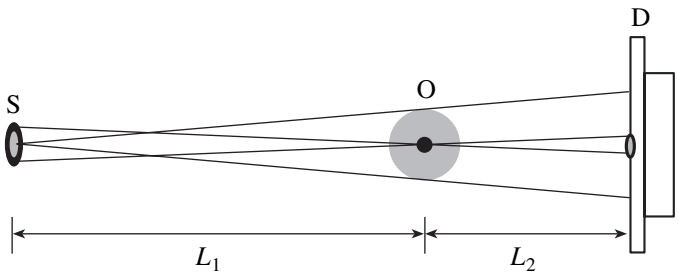

Fig. 1. Experimental layout: source (S), object (O), and position-sensitive detector (D). Converging rays show the source projection equal to the region of averaging the coherent pattern; diverging rays show the object shadow region.

EXPERIMENTAL

The experiment was carried out at the Station for X-ray Crystallography and Materials Science (XCMS) on the 4.6 channel of the source of KCSRNT [13]. The XCMS station is equipped with a vacuum two-crystal monochromator, slit collimators, SR beam monitors, an x-ray detector, and a universal set of goniometric devices necessary to solve problems of x-ray materials science. The station is equipped with dynamic stabilization systems of the spatial position of the SR beam in the extraction channel (the precision is ~10 μm) and the angular position of the second crystal monochromator (precision is ~0.03 arc seconds), which provide necessary conditions for precise x-ray diffraction experiments. Silicon wafers with (111) symmetric reflections were used as crystals monochromators.

The experimental layout is shown in Fig.1. Radiation from the source passed through the monochromator (not shown in the figure) and transilluminated microobjects (a Fresnel ZP and a boric fiber) placed in the same holder. The spatial structure of the wave field intensity was recorded on a high-resolution Kodak film positioned at the ZP focus. The film resolution was no worse than 1 μm per dot. The source–object distance was L_1 = 15.06 m, while the object–film distance depended on the focal length of the used ZPs.

Radiation with a photon energy of 12 keV (wavelength is λ = 1.033 Å) was focused using a round silicon single-crystal ZP with the radius of the first zone r_1 = 12.44 μm and the number of zones N = 242. The ZP aperture and outermost zone size were 387 and 0.4 μm, respectively. The etched region depth and, correspondingly, the zone thickness equaled h = 9 μm. Such a ZP focuses a 12-keV plane wave at a distance $F = r_1^2/\lambda$ = 1.5 m with the efficiency of the order of 20%. With regard to the finite distance L_1 to the source, the focal length L_2 = 1.667 m is determined by the lens formula $L_2^{-1} = F^{-1} - L_1^{-1}$. Figure 2 shows the digitized source and fiber images obtained by scanning films with a pixel size of 0.885 μm.

The source image is shaped as an ellipse strongly elongated along the horizontal axis. Since the image size significantly exceeds the diffraction limit of the dot image, equal to the outermost zone size for the ZP, this image is indeed a real image of the source. The fiber represented a 100-μm-diameter boron cylinder, inside which a 20-μm-diameter tungsten cylinder was placed. The fiber was positioned horizontally; hence, only the vertical intensity distribution is of interest. Although the complex structure of interference fringes cannot be distinguished in the image, the first interference fringe (black) on the fiber edge is clearly pronounced.

The increase in intensity at the fiber edge has the interference (coherent) nature. Because of refraction at the round boundary of the fiber, beams deflect from its axis. At a certain distance after passing through the fiber, these beams interfere with beams that bypassed the fiber. The phase difference between these beams increases with increasing distance from the boundary. When the phase difference is π, a destructive interference arises, and the intensity decreases almost to zero. At a phase difference of 2π, a constructive interference occurs. In this case, the intensity increases almost four times, since the beam amplitudes are summed upon interference, and the intensity is the squared summed amplitude. Therefore, the first two fringes do not com-

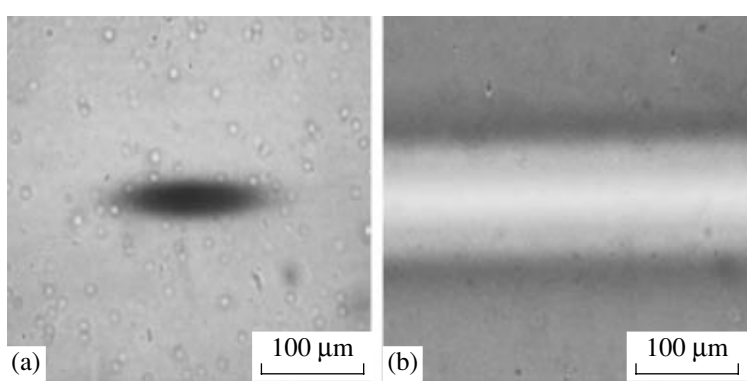

Fig. 2. (a) Source image focused using a zone plate and (b) phase-contrast image of a boric fiber with a tungsten core obtained at the same distance. The x-ray photon energy is 12 keV.

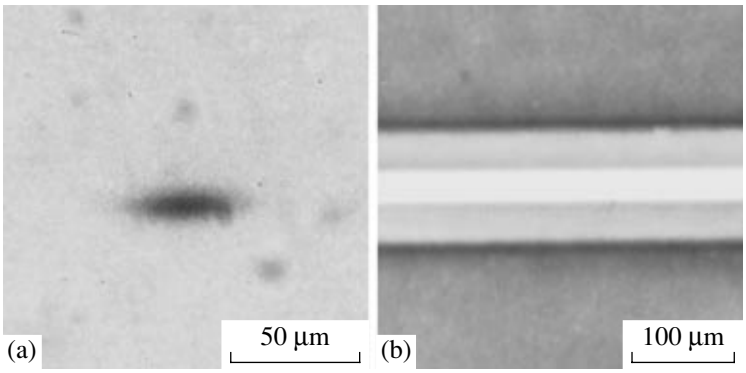

Fig. 3. The same image as in Fig. 2 but for an x-ray photon energy of 8 keV.

pensate each other when the image is smeared by a source of finite transverse sizes. Exactly this situation allowed us to observe the interference increase in the intensity at the fiber edge. The finer effect of a decrease in intensity is not seen by eye but is revealed in mathematical processing. We note that the width of the black fringe is approximately the same as the vertical size of the source image, and this fringe can also be used to measure the effective source sizes.

The focusing of the vertical size of the source was also measured using a linear ZP and another round ZP with differing parameters, and similar results were obtained in these measurements.

Radiation with a photon energy of 8 keV (wavelength is 1.55 Å) was focused using a round ZP with the radius of the first zone r_1 = 8.8 μm and the number of zones N = 122. The aperture of this ZP and the outermost zone size are 194 and 0.4 μm, respectively. This ZP focuses the 8-keV plane wave at the distance $F = r_1^2/\lambda$ = 0.5 m. With regard to the finite distance L_1 = 15.06 m to the source, the focal length L_2 is 0.517 m. Figure 3 shows the source and fiber images obtained by scanning films with pixel sizes of 0.354 and 0.885 μm. The images exhibit similar structures; however, the source image sizes decrease because of a shorter object–film distance, and the interference maximum at the fiber image edges becomes more distinct.

ANALYSIS OF THE RESULTS AND DETERMINATION OF THE SOURCE SIZE

As is known, the distribution of the wave field intensity over coordinates in the focal plane should be known to determine the source size by focusing. In this case, the half-width (FWHM) of this distribution immediately yields the source size after dividing by the geometrical magnification factor equal to $M = L_2/L_1$. However, the problem is that the film exhibits only the blackening D equal to the logarithm of the intensity. Hence, the relative intensity can be calculated by the equation $I_R = \exp(\alpha D - \beta)$, in which the coefficients α and β should be determined independently.

To avoid this problem, we begin an analysis of the results with the fiber image shown in Fig. 3. The vertical cross section near the left edge, averaged over nine horizontal points, was determined from this image. The corresponding dependence of the blackening on the coordinate (micrometers) (with regard to the pixel size) is shown in Fig. 4. This image exhibits two blackening levels. One corresponds to radiation outside the fiber. Because the experimental curve will be compared with the theoretically calculated data, the unit intensity can be associated with this level. Another level is in the region of the cross section that contains no tungsten. The average intensity in this region depends weakly on the source size and must correspond to the theoretical absorbance of boron. For this cross section, the coefficients α = 0.005 and β = 0.4 were determined. It is clear that the former coefficient depends on the film properties and processing method but does not depend on the exposure time, whereas the latter coefficient depends only on the exposure time. We can see in Fig. 4 that the blackening in the shadow region of the tungsten core is

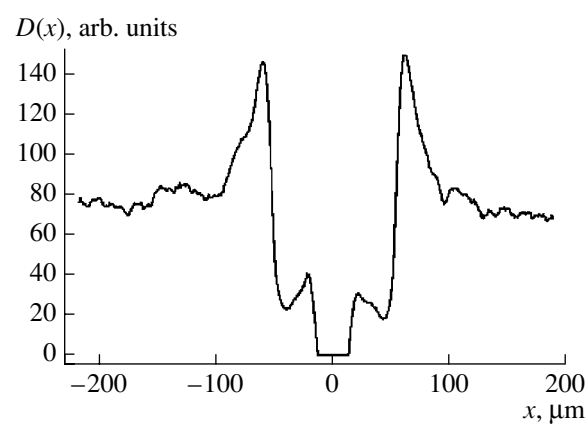

Fig. 4. Dependence of the blackening on the coordinate in the vertical cross section of the boric fiber image for a photon energy of 8 keV.

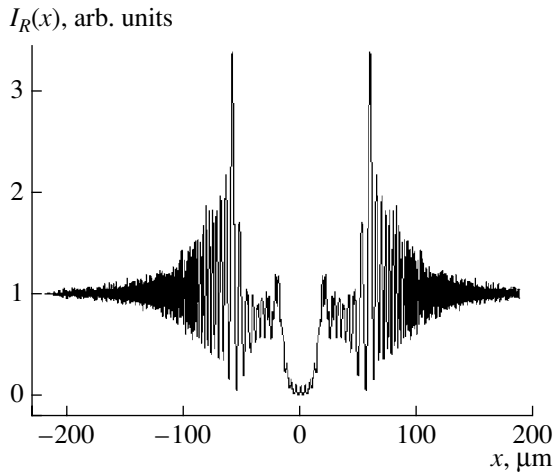

Fig. 5. Relative radiation intensity as a function of the coordinate when a boric fiber is exposed to coherent radiation from a point source at a photon energy of 8 keV.

strictly zero. This is because the exposure time is insufficient. As a result, the blackening in the fiber shadow region does not describe the intensity; that is, it lies outside the dynamic range of the film. However, this is insignificant for determining the source size, since the region of the interference maximum at the image edge is most sensitive.

For comparison with theoretical intensity profiles, we calculated radiation transport for the above experimental parameters. Consider a spherical wave diverging from a point source placed in the optical axis passing through the fiber and detector centers. This wave is modified by the fiber in the geometrical optics approximation, i.e., is simply multiplied by the exponential transmission function that takes into account the wave phase shift due to the optical density of the material and the decrease in the amplitude due to absorption. The maximum phase shift for the boric cylinder of diameter $t = 100$ μm is $\Delta\varphi_B = -28.513$ rad, and the highest absorbance $\mu_B t$ is 0.05. As for tungsten, we should take the values of its parameters minus the values for boron, since tungsten substitutes for boron. The additional phase difference and the absorbance are –32.744 rad and 10, respectively. The further radiation transport through the air between the fiber and the film is determined by the convolution of the wave field in the plane immediately behind the fiber with the Kirchhoff propagator in the paraxial approximation. This theory has been outlined in detail, e.g., in [12].

Figure 5 shows the distribution of the relative radiation intensity calculated for a point source in the same region as the experimental curve, but with a step of 0.25 μm. It is understood from this figure that the fully coherent fiber hologram is rather complex. The maximum period of intensity oscillations is observed near the fiber edge end to be ~7 μm. As the distance from the fiber edge increases, the oscillation period decreases to extremely small sizes. This hologram property allows the size of very small sources to be determined to a high accuracy. At the next stage, we calculated the convolution of the intensity distribution shown in Fig. 5 with the Gaussian distribution with various half-widths corresponding to various source sizes. The theoretical values were interpolated to the same points at which the experimental intensity was determined.

Figure 6 shows six fragments with the same experimental distribution (circles) shown in each of them and theoretical curves calculated for various source sizes from 150 to 500 μm. A comparison of the curves allows the conclusion that the vertical source size is 325 ± 25 μm.

As for the source images obtained with focusing, their vertical cross sections were also measured as blackening curve versus coordinates. Determining the half-width of the blackening curves and dividing it by the magnification factor M, we obtain a value of 360 μm. After the blackening curves were converted into the intensity using the coefficient α determined above, the source size was determined by the above method to be 320 μm. This value correlates very well with the data for the fiber.

DISCUSSION OF THE RESULTS

As follows from the previous section, the method for obtaining a direct image of the source on a film for determining its size is not as simple as it seems at first glance. The film blackening is proportional to the logarithm of the intensity; moreover, it has a limited dynamic range. In the case of small source sizes, both factors cause additional difficulties. First, under strong contrast conditions, the half-width of the logarithmic function is much larger than the half-width of its argument. Second, when the difference in the blackening is large, the dynamic range of the film can be exceeded. Therefore, at small source sizes and a large gain in intensity, position-sensitive detectors with wide dynamic ranges should be used [14]. The situation can be rescued using low-efficiency and, hence, poorly focusing optical elements; however, the diffraction limit of an optical system should be very well known in this case. Moreover, mathematical processing might be required to eliminate the influence of the optical system on the obtained pattern.

However, in the case under consideration, it was found that the half-width of the blackening curve exceeds the half-width of the intensity by only 11%. This raises the problem of determining conditions for the contrast at which such a situation arises. An analysis of this problem in the case of a Gaussian intensity distribution is relatively simple. Let the radiation intensity

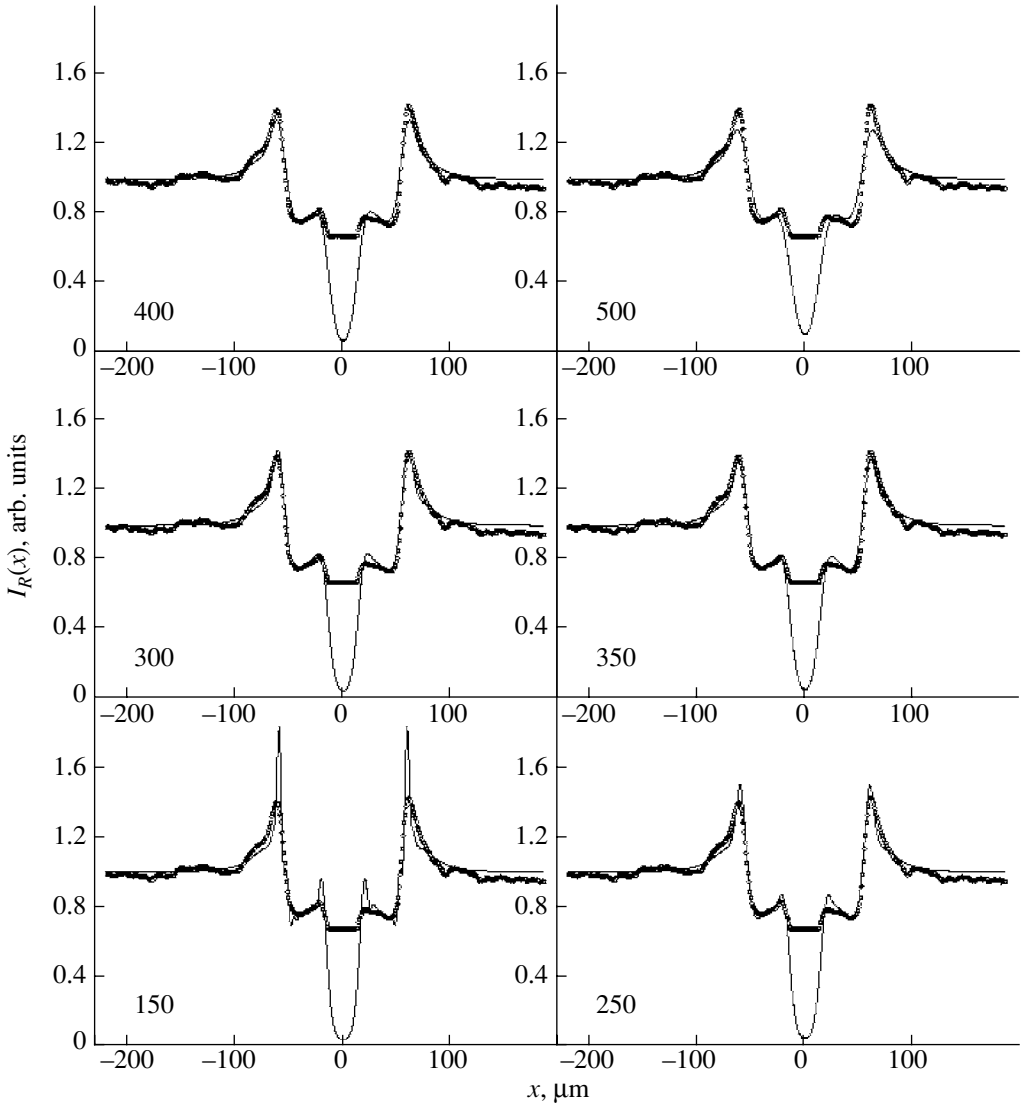

Fig. 6. Comparison of the experimental relative intensity with theoretical curves calculated for various transverse sizes of the source. The source sizes are given on the plots in micrometers.

be described as a function of coordinate x by the expression

$$I_R(x) = \exp(\alpha D(x) - \beta) = A\exp(-a(x/x_0)^2) + B, \quad a = \ln 2, \tag{1}$$

where $D(x)$ is the film blackening. It is clear that the half-width of the curve $I_R(x)$ is equal to $2x_0$. At the same time, the half-width of the blackening curve $2x_1$ can be determined by direct calculations

$$2x_1 = 2x_0 G, \quad G = \left(\frac{\ln C}{\ln 2}\right)^{1/2}, \quad C = 1 + (1 + c)^{1/2}, \quad c = \frac{A}{B}. \tag{2}$$

It follows from formula (2) that the half-width of the blackening curve is always larger than the half-width of the intensity curve, since C is always larger than two. However, the question remains of how large this difference is and what factors determine its value. Since the blackening cannot be negative, the intensity described by the blackening always has a nonzero background, i.e., the minimum value of $B = \exp(-\beta)$ is always larger than zero. The larger the height of the intensity maximum above the background, the larger the degree of broadening is. The function $G(c)$ is shown in Fig. 7. At very small values of c, we can approximately write $G(c) = 1 + 0.18\ c$, but the derivative rapidly decreases with c.

We note that the parameter c is approximately equal to unity in the experimental data on focusing. This determines the slight increase in the half-width

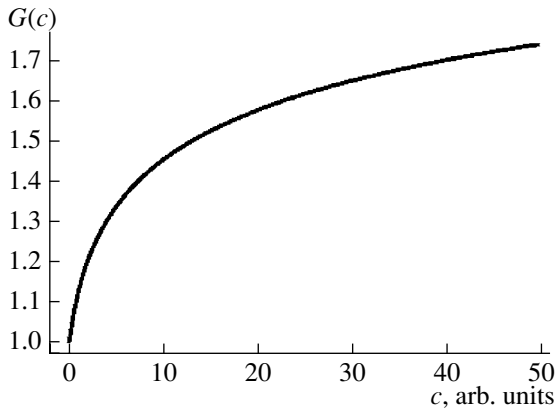

Fig. 7. Universal curve $G(c)$ describing the ratio of the half-widths of blackening and intensity curves as a function of the contrast c.

when the blackening curve is used. The curve obtained above might be used to convert the half-width of the blackening curve into the half-width of the intensity curve at any c. However, the difficulty is that this parameter in terms of the blackening curve is given by

$$c = \frac{A}{B} = \frac{\exp(\alpha D_{\max})}{\exp(\alpha D_{\min})} - 1. \quad (3)$$

Hence, it depends, in any case, on the unknown coefficient α. As for the holographic image of the fiber, the transition from the blackening to the intensity is necessary to achieve an acceptable agreement of the experimental profile with the theoretical calculation.

ACKNOWLEDGMENTS

The authors are grateful to V.N. Korchuganov for maintaining the normal operation of the SR source.

This study was supported by the Russian Foundation for Basic Research, projects no. 03-02-16971, 03-02-17382, 04-02-17363, and 05-02-16702.

REFERENCES

1. A. Snigirev, I. Snigireva, V. Kohn, et al., Rev. Sci. Instrum. **66**, 5486 (1995).
2. C. Raven, A. Snigirev, I. Snigireva, et al., Appl. Phys. Lett. **69**, 1826 (1996).
3. V. G. Kohn, Phys. Scr. **56**, 14 (1997).
4. A. Snigirev, Rev. Sci. Instrum. **66**, 2053 (1995).
5. W. Yun, B. Lai, Z. Cai, et al., Rev. Sci. Instrum. **70**, 2238 (1999).
6. W. Yun, B. Lai, A. A. Krasnoperova, et al., Rev. Sci. Instrum. **70**, 3537 (1999).
7. A. Snigirev, V. Kohn, I. Snigireva, and B. Lengeler, Nature **384**, 49 (1996).
8. B. Lengeler, C. Schroer, M. Richwin, et al., Appl. Phys. Lett. **74**, 3924 (1999).
9. P. Kurapova, S. Feste, M. Gather, et al., Proc. SPIE–Int. Soc. Opt. Eng. **5539**, 38 (2004).
10. C. G. Schroer, B. Lengeler, B. Benner, et al., AIP Conf. Proc. **507**, 340 (2000).
11. V. Kohn, I. Snigireva, and A. Snigirev, Phys. Rev. Lett. **85**, 2745 (2000).
12. V. Kohn, I. Snigireva, and A. Snigirev, Opt. Commun. **198**, 293 (2001).
13. http://www.kcsr.kiae.ru/stations/k4.6.php.
14. A. Koch, C. Raven, A. Snigirev, and P. Spanne, J. Opt. Soc. Am. A **15**, 1940 (1998).